VOL. 10, NO 20, NOVEMBER, 2015 ISSN 1819-6608
ARPN Journal of Engineering and Applied Sciences

www.arpnjournals.com

HARMONIC SIGNAL DETECTION BASED MAGNETIC NANOPARTICLE IMAGING SYSTEM FOR BREAST CANCER DIAGNOSIS

Nurmiza Binti Othman[1], Takashi Yoshida[2] and Keiji Enpuku[2]
[1]BioMEMs Focus Group, Department of Elecronic Engineering, Faculty of Electrical and Electronic Engineering, Universiti Tun Hussein Onn Malaysia, Batu Pahat, Johor, Malaysia
[2]Graduate School of Information Science and Electrical Engineering, Kyushu University, Fukuoka, Japan
E-Mail: nurmiza@uthm.edu.my

ABSTRACT

An imaging method based on the second harmonic (B_{s2}) signal detection from the magnetic nanoparticles (MNPs) has been developed to be applied for the Sentinel Lymph Node (SLN) detection during the breast cancer diagnosis. SLN can be detected by measuring the magnetic field signal of the injected MNPs tracer inside the body, instead of the conventional methods such as radioisotopes and/or blue dye tracers. The position and amount of MNPs accumulated at the SLNs are determined based on the magnetic field map measurement. The developed system can detect until 100-µg MS1 type-MNP sample located at a depth of 30 mm from the detection coil. Future improvements on the system and MNPs selection could further increase the detection sensitivity. MNPs that are accumulated at the deeper position under the body's surface can be detected and distinguished with higher spatial resolution.

Keywords: magnetic nanoparticle, harmonic signal, breast cancer, sentinels lymph node, medical imaging, nonlinear *M-H* curve.

INTRODUCTION

Magnetic tracers, which are composed of polymer-coated nanoparticles (MNPs), may offer some attractive possibilities in biomedical applications such as hyperthermia, drug delivery, immunoassay etc. (Q. A. Pankhurst *et al*., 2009). Their magnetic properties can be easily controlled using external field excitation. In this way, they can be used to extend novel techniques, especially those for magnetic particle imaging (MPI) (B. Gleich *et al*., 2005), (J. B. Weaver *et al.,* 2008), (T. F. Sattel *et al*., 2009), (P. W. Goodwill *et al*., 2012).

Magnetic particle imaging is a new technique for the quick 3D imaging of the distributions of polymer-coated MNPs, especially in in-vivo diagnostic procedures for detecting cancer cells in the human body. MPI can be used for Sentinel Lymph Node (SLN) biopsy (K. Gräfe *et al*., 2012). SLN, the first lymph node in which cancer cells appear before they spread to other lymph nodes. To detect SLN, MNPs can be used as tracer instead of conventionally used radioisotopes or blue dye tracers. The position and amount of MNPs accumulated at the SLN are determined by measuring the magnetic field signal of the injected MNPs inside the body. Therefore, SLN position can be determined for breast cancer staging through the MNPs imaging.

To this end, a 100-µg MNPs sample accumulated at a depth of 30 mm under the body surface should be detected (S. Tanaka *et al*., 2001), (M. Abe *et al*., 2012), (K. H. Song *et al*., 2009). Hence, a highly sensitive imaging system that can accurately estimate the position of the MNP sample is needed. It is also necessary to distinguish the MNPs accumulated in an SLN from those accumulated in an adjacent lymph node with high spatial resolution.

In this work, an MPI system that detects the second harmonic signal (B_{s2}) from MS1, the fractionated MNPs of Resovist, has been developed. Since harmonic signals have different frequencies with the excitation frequency, interference from the excitation field can be significantly decreased, and detection sensitivity can be improved. In addition, a magnetic signal processing method using the singular value decomposition (SVD) has been employed to obtain higher spatial resolution image of the MNP density distribution, reconstructed from the contour map of the measured magnetic field.

BREAST CANCER DIAGNOSIS

Sentinel lymph node biopsy

Sentinel Lymph Node Biopsy (SLNB) is a process of localization, dissection, and histological examination of the sentinel lymph node to study the status of the entire lymphatic system for breast cancer staging. Figure-1 shows the lymphatic system draining the breast, indicating tumor and SLN. A lymph node appears as a bean-shaped organ, whose size is ranging from a few mm to 1 - 2 cm order. It acts as a filter to clean lymph as it passes through the node.

Cancer cells migrate and spread via the lymphatic system. They migrate from tumor and are carried away by the fluid in lymphatic system. They are mostly trapped in one or more than 500-600 nodes that are distributed around the lymphatic system throughout the body. Therefore, the spread of cancer cells from local tumor to adjacent cells, tissues, or lymph nodes, or to multiple

tumors at distant sites is indicated during the cancer staging of SLNB. The staging process is based on whether the cancer is invasive or non-invasive, the size of the tumor, how many lymph nodes are involved, and if it has spread to other parts of the body.

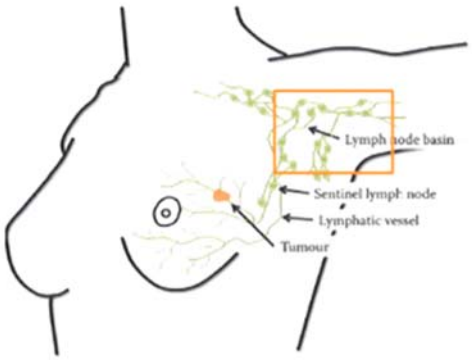

Figure-1. Lymphatic system draining the breast, indicating tumor and sentinel lymph node.

SLNB is an important process of finding out how widespread a cancer is when it is diagnosed. Depending on the results of the biopsy, doctor will decide whether patients may undergo some other imaging tests such as a chest x-ray, mammograms of breasts, bone scans, Computed Tomography (CT) scans, Magnetic Resonance Imaging (MRI), and/or Positron Emission Tomography (PET) scans.

Prior to SLNB, axillary lymph node dissection (ALND) has been used where most of lymph nodes at the axillary region are removed (indicated by the squared area in Figure 1). Short term effect of lymphoedeme, and long term effects of nerve damage are inevitable. Because SLNBs involve less extensive surgery and the removal of fewer lymph nodes than standard ALND, the potential for adverse effects, or harms, is lower. Besides, clinicians can easily determine the cancer stage by only smaller incisions involved in removing the lymph nodes.

The procedural sequence for SLNB using a generic tracer is elaborated as follows. First, tracer is injected at the primary tumor site. Then tracer follows drainage path of tumor to nearest lymph nodes. The draining lymph node is detected with sensor at the body surface. Surgeons will remove additional regional lymph nodes if dissected lymph node shows signs of malignancy. Conversely, the remaining regional lymph nodes will not be removed if they show no signs of malignancy.

Conventional tracers which have been used for SLNB generally involve a so-called "combined technique" for SLNB: the injection of technetium-sulphur-colloid ^{99m}Tc together with isosulfan blue or Patent blue into the tumor region. The localization of these kinds of tracer is done by using a gamma probe to locate the lymph nodes receiving primary drainage from tumor region via the lymphatic vessels. Lymph nodes containing radioactive tracers are judged as "sentinel" and are then removed for examination. Besides, blue dye assists in post-incision localization where it stains the lymph nodes into blue color. Hence, lymph nodes that are blue when identified with surgeon's naked eye is judged as SLNs.

While effective, these tracers come along with several inevitable limitations such as the exposure of patient and clinicians to ionizing radiation, limitation in its availability to proximal centers due to their short shelf life, waste disposal problems, handling license mandatory, etc. Therefore, the use of MNPs as promising new tracer to replace the "combined-technique" in SLNB can be expected to address these problems.

MNP imaging for SLNB

MNPs have some features that can be exploited as the most suitable tracer to replace the conventional ones. First, MNPs can be externally detected in tissue before the incision, however, by using a much simpler detection system instead of gamma sensor. Second, they are of similar dimension to the radioactive colloid, and lastly, their brown-black appearance when concentrated at SLN, acts as a visual stain which can be detected by surgeon visually, as similar as that of blue dye detection.

Superparamagnetic iron oxide MNPs such as maghemite (γFe_2O_3) and magnetite (Fe_3O_4) are coated by biocompatible polymers: e.g. dextran and carboxydextran, especially for the purpose of in vivo imaging. They exhibit super paramagnetism as response to an external magnetic field excitation while sustaining zero magnetic remanence when no magnetic field is applied. These features make them ideal for SLNB application as they are prevented from agglomerating while being migrated via the lymphatic system in the absence of magnetic field.

Injected MNPs respond diversely in the lymphatic system, depending on their diameter size. MNPs with a diameter in the tens of nm are the most ideal tracer for SLNB. Note that the size of conventionally used SLNB tracer of ^{99m}Tc is a few tens of nm, therefore, development of MNPs for the purpose of SLNB should be focused on an MNP having a size similar to the ^{99m}Tc, so that the dynamics of the MNPs which migrating through lymphatic system should be commensurate.

SLNB using MNPs tracer goes similar procedure with the one using the "combined-technique". In other words, it is preferable to maintain the same surgical procedure while changing the underlying detection method: replacing the radioisotope tracer and gamma probe with MNPs tracer and simpler magnetometer. Since the mean depth of SLNs in human body is 12 ± 5 mm (standard deviation, from the top surface of SLNs to the body surface), it is necessary to demonstrate the clinical depth capability of the imaging system based on MNP

tracer detection (K. H. Song *et al*., 2009). In addition, an imaging system that has a spatial resolution better than 25 mm for lymph nodes in the axilla region is recommended to separate MNPs tracers accumulating at neighboring lymph nodes (H. Wengenmair *et al*., 2005).

MAGNETIC NANOPARTICLES FOR MAGNETIC PARTICLE IMAGING

Magnetic response of MNPs

Figure-2 shows a schematic drawing of a spherical MNP consists of a magnetic core with biocompatible coating for biomedical applications. It is well known that the magnetic properties of MNPs show the super-paramagnetic behavior and can be expressed by the Langevin function (S. Chikazumi, 1964). In the absence of external magnetic field, the magnetic moment in each of MNPs randomly rotates owing to the thermal noise. Accordingly, the direction of the magnetic moment becomes random, and the mean value of the magnetic

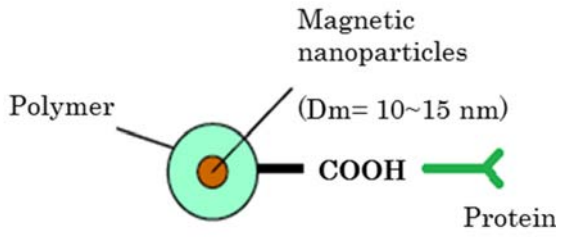

Figure-2. Schematic drawing of a spherical MNP consists of a magnetic core with biocompatible coating for biomedical applications.

moment of the MNPs becomes zero.

However, when MNP is magnetized under external field excitation, H, the magnetic moments in the MNPs tend to align in the direction of the H. The mean magnetic moment of MNPs in the direction of H, which is defined as $< m >$, can be described by

$$\frac{\langle m \rangle}{m} = L\left(\frac{mH}{k_B T}\right) = \coth\frac{mH}{k_B T} - \frac{k_B T}{mH} . \quad (1)$$

L indicates the Langevin function, m is the magnetic moment of the MNPs, k_B is the Boltzmann constant, and T is the absolute temperature.

When an external field consisting of the DC bias field H_{DC} and the AC field $\sqrt{2}H_{AC}\cos(\omega t)$ is applied,

$$\frac{\langle m \rangle}{m} = \coth\left[\frac{H_{DC} + \sqrt{2}H_{AC}\cos(\omega t)}{k_B T / m}\right] - \frac{k_B T / m}{H_{DC} + \sqrt{2}H_{AC}\cos(\omega t)} \quad (2)$$

By expanding the right-hand side of equation. (2) into a Fourier series, the n-th harmonic signal from the MNPs can be obtained,

$$\frac{\langle m \rangle_n}{m} = 2\omega\int_0^{1/\omega} L\left(\frac{H_{DC} + \sqrt{2}H_{AC}\cos(\omega t)}{k_B T / m}\right)\cos(n\omega t)dt . \quad (3)$$

Towards better MPI: New MNPs with higher nonlinearity in magnetization

Different aspects play significant roles to assure the image quality in MPI. In addition to the high sensitivity detection hardware and an excellent image processing method, it is important to characterize MNPs which produce the largest harmonic signals for MPI.

As the imaging system utilizes harmonic signals, it is important to select MNPs that can generate strong harmonic signals. However, MNPs show a wide variety of magnetic properties, depending on their magnetic moment m and anisotropy energy E_B (T. Yoshida *et al*., 2012). Using several evaluation methods such as harmonic spectrum measurement, M-H curve measurement, and AC susceptibility measurement, a clear quantitative relationship between several important parameters for harmonic signals contribution from the several types of MNPs: magnetic moment m and anisotropy energy E_B distributions were successfully established. They showed that Resovist had the richest harmonics spectrum, when compared to other MNPs that have been investigated.

Resovist had a wide range of magnetic properties distribution depending on the various particle sizes inside the MNPs. It is understood from the report that larger particles have a significant impact on the harmonic signal

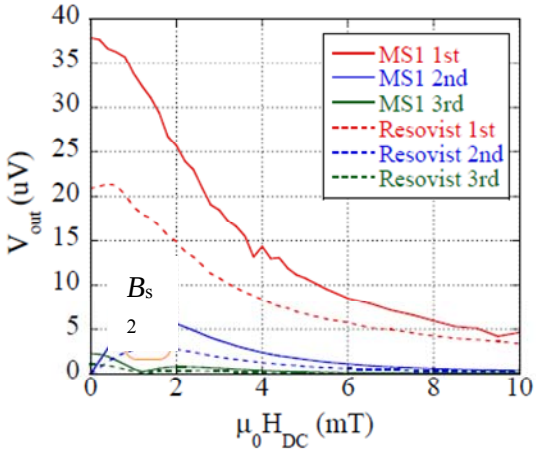

Figure-3. Comparison of the magnitude of the second harmonic component of MS1 and Resovist.

generation from the MNPs. Thus, MNPs composed of only large part of the particle size in Resovist is considered to

produce more harmonics with larger magnitude than the original Resovist. One type of MNP sample known as MS1 having a diameter is 59 nm was obtained by extracting only a large part of the particle size in the Resovist (T. Yoshida *et al*., 2013), (N. B. Othman *et al*., 2014).

Using the MS1 sample, the magnitude of the harmonic signal from Resovist and MS1 sample were measured for comparison. Both samples were diluted with glycerol. Figure 3 shows a comparison of the magnitude of the second harmonic component of MS1 and Resovist. Approximately two times larger signal could be obtained from the second harmonic signal detected from the MS1 sample. Therefore, it can be presumed that a clearer contour map of B_{s2} signal could be obtained if MS1 is used as the imaging sample, instead of Resovist.

HARMONIC SIGNAL-BASED MAGNETIC NANO-PARTICLE IMAGING

MNP imaging system

In this work, an MNP imaging system suitable for the SLN biopsy has been designed, constructed and tested using the MS1 sample. A harmonic signal detection-based MNP imaging system especially for a narrow band MPI was developed to obtain a high signal-to-noise ratio (SNR) signal for image reconstruction. From the experimental work on the study of the harmonic signal components of Resovist, an MNP imaging system employing the B_{s2} signal detection of MNPs was proposed (N. B. Othman, 2012), (N. B. Othman, 2013).

Figure-4 shows the MNP imaging system that was developed. I_{DC} = 0.8 A and I_{AC} = 0.8 A with frequency of 19.3 kHz was applied to magnetize MNPs, however, in this case MS1 samples were used to replace Resovist. The amplification of the magnetic signal was done by designing a resonant circuit for both of the pickup coil and the excitation coil. An immobilized MS1 samples (MS1 diluted with glycerol) containing of 100 µg of Fe was placed into a cell with a diameter of 6 mm and a height of 5 mm. Details of the measurement apparatus and sample preparation are given elsewhere.

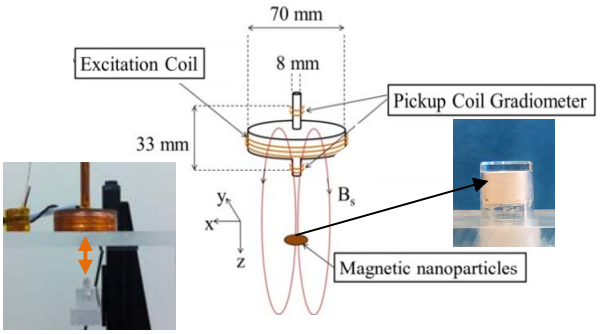

Figure-4. MNP imaging system using the MS1 sample.

First, the sensitivity of the imaging system was explored. The present system could detect a 100-µg immobilized MS1 sample located at z = 30 mm with the SNR as high as 18. This detection sensitivity is adequate for the SLN detection using MNPs.

Next, the localization of MNPs in the xy plane could be obtained directly from the contour map of the B_{s2} signal measured in z axis, B_z. The magnetic field from the MS1 sample was measured and the detected signal was plotted as a contour map in order to identify the position of the MNPs. To this end, the sample was moved in the x direction from x = -40 mm to 40 mm at a speed of 20 mm/s. The harmonic signal B_{s2} was detected at intervals of 2 mm from y = -40 mm to 40 mm. $x = y = 0$ when the sample was positioned at the center of the pickup coil.

Figure-5(b) shows the measured magnetic field map when one MNP sample of MS1 diluted with glycerol was located at z = 30 mm. Similar measurement was done to the Resovist sample diluted with glycerol for comparison. The result is shown in Figure-5(a). It can be seen that clearer contour map was successfully obtained for the case of (b), where the peak value at $x = y = 0$, corresponds to the real position of the MS1 sample located under the body surface. Therefore, the real position of one MNP sample could be estimated directly from the contour map.

On the other hand, Figure-6 shows the measured contour map when two MS1 samples of similar weight (100 µg) were located at z = 30 mm under the pickup coil and were separated by Δx = 20 mm. This simulates the situation where MNPs are accumulated at the SLN and the adjacent lymph node. The signal field shows a broad peak; therefore, it is difficult to clearly distinguish the two samples using the contour map. To improve the spatial resolution of the estimated position, the measured contour map of B_{s2} was analyzed using a mathematical technique of SVD as will be introduced in the next section.

Singular value decomposition (SVD) for higher spatial resolution image

A signal processing method has been developed to obtain a high spatial resolution image reconstructed from the measured magnetic field of B_z. Despite of the high sensitivity detection for one MNP sample, it was very challenging to distinguish two MNP samples located at $z \geq 15$ mm and separated by Δx = 20 mm directly from the contour map of B_z magnetic field (Figure-6). Therefore, an additional analysis should be done on the magnetic field signal obtained from the measurement so that better spatial resolution can be improved for excellent image reconstruction.

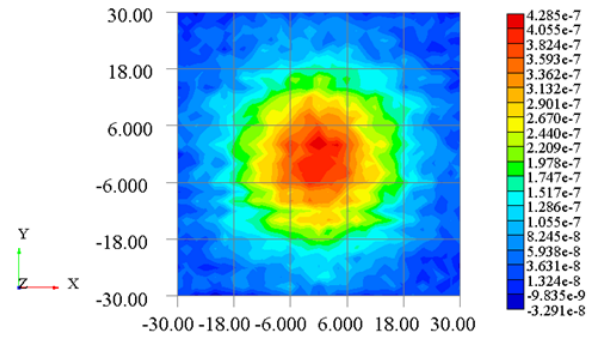

(a)

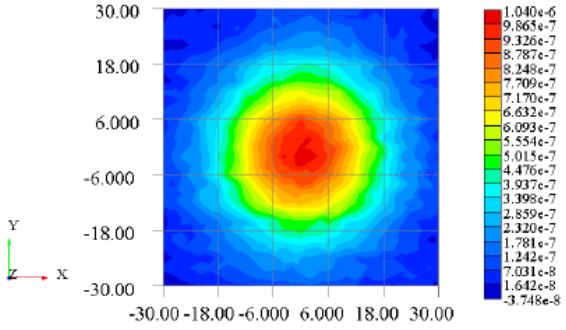

(b)

Figure-5. Contour map of B_z signal detected from one sample of (a) Resovist and (b) MS1 MNP.

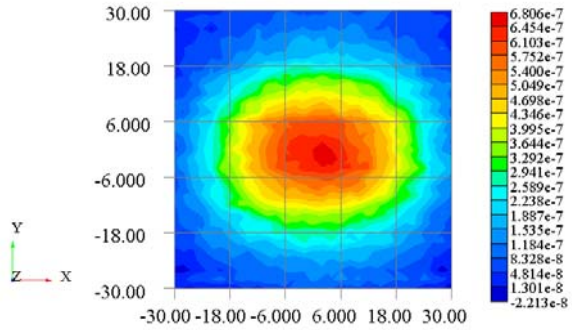

Figure-6. Contour map of B_z signal detected from two MS1 samples. z = 30 mm and Δx = 20 mm.

A mathematical calculation technique known as singular value decomposition (SVD) was employed to analyze the B_z (K. Enpuku *et al*., 2008). This technique enables the contour map $B_z(x,y)$ measured at z = 0 to be converted to the MNP density distribution $n(x,y)$ at a given sample depth z. The estimated position of the two MNP samples could be considerably distinguished with better spatial resolution using the proposed technique.

Magnetic field signals measured experimentally, denoted as V_m obey the following relationship of

$$V_m = Ac \,. \tag{4}$$

V_m could be obtained from a correlation between a system matrix A and the distribution of the MNP sample's concentration c which corresponds to the signal generation. Then, a system matrix A is introduced as $A = USV^T$. Therefore, Equation. (4) can be rewritten as

$$V_m = \left(USV^T\right)c \,. \tag{5}$$

c can be determined from the measured magnetic field vector V_m by an inverse matrix calculation of

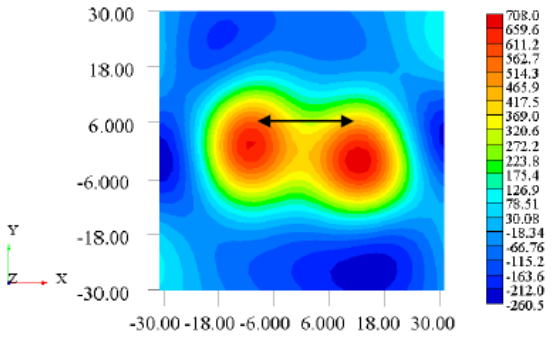

Figure-7. Contour map of $n(x,y)$ for two MS1 samples. z = 30 mm Δx = 20 mm.

$$c = \left(VS^{-1}U^T\right)V_m \,. \tag{6}$$

Using the SVD analysis, a MNP density distribution of $n(x,y)$ could be obtained as shown in Figure-7.

In this case, two MS1 samples of similar weight (100 µg of iron) were located at z = 30 mm below the detection coil, and were separated by Δx = 20 mm. Two maxima in the particle concentration can be obtained, and the positions for the maxima agreed with the real positions of the MNPs. Therefore, two MNP samples that were not clearly observed in Figure 6 could be easily distinguished by using this method.

Future works

The performance of the proposed MNP imaging system and the signal processing of SVD analysis still got a lot of room for improvement.

First, a fast scanning of magnetic signal over the imaging area is needed to obtain a high temporal resolution signal for image reconstruction. The magnetic signal from magnetized MNPs tends to decay over measurement time due to the drop of bias field magnitude in the excitation circuit during the measurement. Further improvement on excitation circuit, e.g. by taking thermal noise effect into account, will need to be performed in the future.

Next, an additional signal processing method of SVD was used to analyze the experimental magnetic signal. Magnetic field map was converted to the MNP density distribution map via the SVD analysis. With this method, the present MNP imaging system could distinguish until two MNP samples located at z= 30 mm and were separated by Δx= 20 mm with high spatial resolution. Future work should concentrate on investigating the limitation of the SVD analysis for the magnetic signal from deeper-lying MNPs under the body's surface.

Finally, numerical simulation results of the SVD analysis indicate negative values of particle concentration in the MNP density $n(x,y)$ distribution map (Figure 7). This 'negative concentration' can be considered as an unacceptable phenomenon in physics and logical thinking. Therefore, this finding may suggest an opportunity for further research to find new solution to address the problem faced during the mathematical calculation.

CONCLUSIONS

An MNP imaging system that uses the B_{s2} signal detection has been developed especially for the in vivo applications. A 100-µg of MS1, the fractionated MNPs of Resovist, located at z = 30 mm was successfully detected from the present system. Besides, the positions of two MS1 samples separated by Δx = 20 mm at z = 30 mm were also clearly distinguished with the assist of a mathematical calculation technique known as singular value decomposition method. This simple MNP imaging system will be useful for medical applications especially for the SLN detection in breast cancer diagnosis.

ACKNOWLEDGEMENT

This research was conducted with financial support by Short Term Grant (STG) Vot Number U117.

REFERENCES

B. Gleich and J. Weizenecker. 2005. Tomographic Imaging Using the Nonlinear Response of Magnetic Particles. Nature, 435, pp. 1214-1217.

H. Wengenmair, and J. Kopp, and J. Sciuk. 2005. Quality Criteria of Gamma Probes: Requirements and Future Developments. The Sentinel Lymph Node Concept. pp 113-125.

J. B. Weaver, A. M. Rauwerdink, C. R. Sullivan, and L. Baker. 2008. Frequency Distribution of the Nanoparticle Magnetization in The Presence of A Static As Well As A Harmonic Magnetic Field. Med. Phys., 35, pp. 1988-1994.

K. Gräfe, T. F. Sattle, K. Lüdtke-Buzug, D. Finas, J. Börgert, and T. M. Buzug. Springer, 2012. Magnetic-Particle-Imaging for Sentinel Lymph Node in Breast Cancer. Springer Proc. Phys. 140, Second International Workshop on Magnetic Particle Imaging, ed. by T. M. Buzug and J. Borgert, Germany, pp.237-241.

K. Enpuku, T. Tanaka, Y. Tamai, F. Dang, N. Enomoto, J. Hojo, H. Kanzaki, and N. Usuki. 2008. Size Distribution of Magnetic Marker Estimated From AC Susceptibility in Solution for Biosensor Application. Jpn. J. Appl. Phys., 47, pp. 7859-7865.

K. H. Song, C. Kim, C. M. Cobley, Y. Xia, and L. V. Wang. 2009. Near-infrared Gold Nanocages as a New Class of Tracers for Photoacoustic Sentinel Lymph Node Mapping on a Rat Model. Nano Lett., 9, pp.183-188.

M. Abe, T. Ueda, T. Masaki, Y. Kitamoto, N. Matsushita, and H. Handa. 2012. Detecting Ferrite Nanobeads for Sentinel Lymph Node Mapping with a Highly Sensitive Hall Differential Magnetic Field Sensor. J. Phys.: Conf. Ser., 352, 012015.

N. B. Othman, T. Tsubaki, T. Yoshida, K. Enpuku, and A. Kandori. 2012. Magnetic Nanoparticle Imaging Using Harmonic Signals, IEEE Trans. Magn., 48, pp. 3776-3779.

N. B. Othman, T. Tsubaki, D. Kitahara, T. Yoshida, K. Enpuku, and A. Kandori. 2013. Magnetic Nanoparticle Imaging Using Second Harmonic Signals for Sentinel Lymph Node Detection. J. Magn. Soc. Jpn., 37, pp. 295-298.

N. B. Othman, T. Tsubaki, D. Kitahara, T. Yoshida, and K. Enpuku. 2014. Harmonic Signal Analysis for Magnetic Nanoparticle Imaging. J. Japan Soc. of Powder and Powder Metallurgy.

P. W. Goodwill, E. U. Saritas, L. R. Croft, T. N. Kim, K. M. Krishnan, D. V. Schaffer, and S. M. Conolly. 2012. X-space MPI: Magnetic Nanoparticles for Safe Medical Imaging. Adv. Mater., 24, pp. 3870-3877.

Q. A. Pankhurst, N. T. K. Thanh, S. K. Jones, and J. Dobson. 2009. Progress in Applications of Magnetic Nanoparticles in Biomedicine. J. Phys. D, 42.

S. Chikazumi. Wiley: 1964. Physics of Magnetism, New York.

S. Tanaka, A. Hirata, Y. Saito, T. Mizoguchi, Y. Tamaki, I. Sakita, and M. Monden. 2001. Application of High Tc SQUID Magnetometer for Sentinel-lymph Node Biopsy. IEEE Trans. Appl. Supercond., 11, pp. 665-668.

T. F. Sattel, T. Knopp, S. Biederer, B. Gleich, J. Weizenecker, J. Borgert, and T. M. Buzug, Single-sided Device for Magnetic Particle Imaging, J. Phys. D, Volume 42, (2009), 022001.

T. Yoshida, N. B. Othman, T. Tsubaki, J. Takamiya, and K. Enpuku. 2012. Evaluation of Harmonic Signals for the Detection of Magnetic Nanoparticles. IEEE Trans. Magn., 48, pp. 3788-3791.

T. Yoshida, N. B. Othman, and Keiji Enpuku. 2013. Characterization of Magnetically Fractionated Magnetic Nanoparticles for Magnetic Particle Imaging. Journal of Applied Physics, 114.